Planar Hall Effect in the Charge-Density-Wave $Bi_2Rh_3Se_2$

Mingju Cai(蔡明桔)[1], Zheng Chen(陈正)[2], Yang Yang(杨扬)[2], Xiangde Zhu(朱相德)[2], Haoxiang Sun(孙浩翔)[3], Ankang Zhu(朱安康)[4*], Xue Liu(刘学)[1], Yuyan Han(韩玉岩)[2*], Wenshuai Gao(高文帅)[1*], and Mingliang Tian(田明亮)[2,5]

[1]*Institutes of Physical Science and Information Technology, Anhui University, Hefei 230601, China*
[2]*Anhui Key Laboratory of Low-energy Quantum Materials and Devices, High Magnetic Field Laboratory, Hefei Institutes of Physical Science, Chinese Academy of Sciences, Hefei 230031, China*
[3]*Stony Brook Institute at Anhui University, Anhui University, Hefei 230601, China*
[4]*School of Mathematics and Physics, Bengbu University, Bengbu 233030, China*
[5]*School of Physics and Optoelectronics Engineering, Anhui University, Hefei 230601, China*

(Received 9 April 2024; accepted manuscript online 21 June 2024)

We systematically investigate in-plane transport properties of ternary chalcogenide $Bi_2Rh_3Se_2$. Upon rotating the magnetic field within the plane of the sample, one can distinctly detect the presence of both planar Hall resistance and anisotropic longitudinal resistance, and the phenomena appeared are precisely described by the theoretical formulation of the planar Hall effect (PHE). In addition, anisotropic orbital magnetoresistance rather than topologically nontrivial chiral anomalies dominates the PHE in $Bi_2Rh_3Se_2$. The finding not only provides another platform for understanding the mechanism of PHE, but could also be beneficial for future planar Hall sensors based on two-dimensional materials.

DOI: 10.1088/0256-307X/41/7/077303

Quantum materials are a research hotspot in condensed matter physics for their unique characteristics.[1] Numerous quantum materials have been discovered and extensively studied, including graphene,[2] superconductors such as AV_3Sb_5 (A = K, Rb, Cs),[3] UTe_2,[4] topological semi-metals such as $PtBi_2$,[5,6] ZrSiS,[7] and so on. Lately, two-dimensional ternary chalcogenides, such as $PaTaSe_2$,[8,9] $SnTaS_2$,[10,11] and $InTaSe_2$,[12] have attracted a great deal of attention by their unique architecture, novel physical characteristics, and promising potential application in nanodevices.[13] Recently, the ternary chalcogenide $Bi_2Rh_3Se_2$ was closely investigated for its fancy charge-density-wave and superconductivity. $Bi_2Rh_3Se_2$ belongs to one member of the quasi-two-dimensional ternary chalcogenides $A_2M_3X_2$ (A = Sn, Pb, In, Tl and Bi; M = Co, Ni, Rh and Pd; X = S and Se), containing one-dimensional M–M chains.[14–16] $Bi_2Rh_3Se_2$ is a type-Ⅱ superconductor with a superconducting transition temperature of 0.7 K. The electrical resistivity, magnetic susceptibility, thermoelectric power, sample length change, and x-ray diffraction measurements reveal that this compound is in the CDW state below 240 K.[14] However, the pressure effect and electron diffraction measurements carried out by Yang *et al.* dispute that the anomalous transition near 240 K is a structural rather than a CDW phase-transformation.[16] To address this issue, the spectroscopy experiments performed by Meng *et al.* [17] and Wang *et al.* [18] clearly reveal the formation of an energy gap with associated spectral change only at low energies, yielding strong evidence for a CDW phase transition at 240 K. Furthermore, angle-resolved polarized Raman spectroscopic measurements further reveal the in-plane anisotropic electron-phonon coupling and CDW transition in $Bi_2Rh_3Se_2$.[19] So far, most of the studies focus on the spectroscopy experiments and pressure effect, the magnetotransport properties, especially the in-plane electrical transport properties of $Bi_2Rh_3Se_2$ are still lacking, more studies are urgently needed to understand its physical properties comprehensively.

In this work, we synthesized the intercalated transition metal $Bi_2Rh_3Se_2$ single crystals, and performed systematic in-plane transport measurements. When rotating the field within the plane of sample, distinct angle dependence of planar Hall resistance accompanied with anisotropic longitudinal resistance is observed. Further analysis reveals that the planar Hall effect (PHE) is mainly caused by anisotropic orbital rather than topological chiral anomaly. The findings suggest that $Bi_2Rh_3Se_2$ provides another platform for understanding the physical mechanisms of PHE and potential low-dimensional sensor applications.

$Bi_2Rh_3Se_2$ single crystals were synthesized by employing the method described in previous reports.[20] An optical photograph of millimeter sized $Bi_2Rh_3Se_2$ single crystal is shown in the inset of Fig. 1(c) shows. The x-ray diffraction (XRD) patterns were collected from a Rigaku-TTR3 x-ray diffractometer using the high intensity graphite monochromatized Cu K_α radiation. The measurement of Hall and longitudinal resistances employs a standard six-contact method via a 9-Tesla physical prop-

*Corresponding authors. Email: zak@bbc.edu.cn; yyhan@hmfl.ac.cn; gwsh@ahu.edu.cn
© 2024 Chinese Physical Society and IOP Publishing Ltd

erties measurement setup (PPMS) from Quantum Design Inc., where the magnetic field applied either orthogonal or aligned with the crystal (00l) plane. Energy dispersive spectroscopy (EDS) was carried on an Oxford X-MAX electron spectrometer.

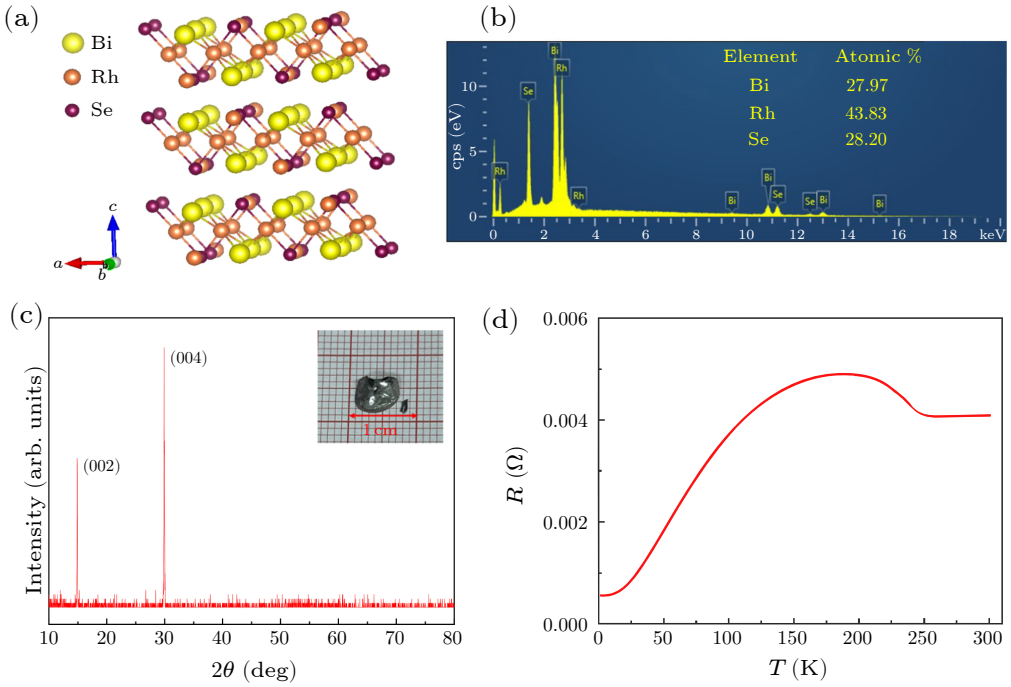

Fig. 1. (a) Crystal structure of $Bi_2Rh_3Se_2$. (b) Energy dispersion spectroscopy (EDS) of $Bi_2Rh_3Se_2$ composite crystal, showing stoichiometric ratio. (c) X-ray diffraction spectra obtained from the (00l) face of $Bi_2Rh_3Se_2$ single crystal. Inset: an optical photograph of the $Bi_2Rh_3Se_2$ single crystal. (d) Temperature-dependent resistance of $Bi_2Rh_3Se_2$ single crystal.

The space group of $Bi_2Rh_3Se_2$ single crystals is $C12/m1$ with a phosphorene-type structure.[19] Formation of a virtually two-dimensional, or quasi-2D, layered configuration is evident in Fig. 1(a). Figure 1(b) shows the EDS of a synthetic crystal. The stoichiometric ratio of Bi : Rh : Se was determined to be 27.97% : 43.83% : 28.20%. Figure 1(d) shows the temperature-dependent resistance of the $Bi_2Rh_3Se_2$ single crystal at zero magnetic field, a distinct curved bulge corresponding to a CDW transition signal near 240 K is observed upon cooling, which is consistent with the previous report.[14] All the results indicate the high quality of the $Bi_2Rh_3Se_2$ samples.

Figure 2(a) shows the magnetic field dependence of the magnetoresistance (MR) at different temperatures when the magnetic field is perpendicular to ab plane. We note that $Bi_2Rh_3Se_2$ single crystals perform quasi-parabolic MR in a low field range and linear MR at high fields without any sign of saturation. At present, the linear magnetorheological behavior in different materials is mostly not well understood, but there are several main mechanisms to explain the linear MR effect.[21–25] One of them is the Abrikosov theory, which is applicable in the presence of linear dispersion. Linear MR is observed when all electrons are populated to the lowest Landau level, that is, the quantum limit is satisfied.[21,23,25] However, Abrikosov's theory is not applicable in the case of $Bi_2Rh_3Se_2$, since there is no conclusive evidence that the magnetic field pushes it to the quantum limit. Furthermore, when the current and magnetic field are parallel to each other, the compensating carrier mechanism normally works nicely for compensating semimetals.[22] The linear magnetoresistance in $Bi_2Rh_3Se_2$ cannot be adequately explained by this mechanism, as it dominates in the case of a perpendicular magnetic field. Figure 2(b) shows the MR curves at different angles as the magnetic field rotates from the c-axis to the ab plane, and the projection is always parallel to the current. The measurement schematic diagram is shown in the inset of Fig. 2(b). For $Bi_2Rh_3Se_2$, the MR varies with each angular displacement, yet there is an absence of notable negative magnetoresistance (NMR) when the orientation of the magnetic field aligns with the flow of current ($\varphi = \pi/2$). Figure 2(c) shows the normal Hall resistance of $Bi_2Rh_3Se_2$ at different temperatures when the magnetic field is perpendicular to ab plane. Over the entire temperature range from 2 K to 300 K, the Hall resistance has a linear relationship with approximately negative slope, indicating that electron-type carriers dominate the transport in $Bi_2Rh_3Se_2$. As depicted in Fig. 2(d), the variations in carrier concentration and mobility in correlation with temperature are derived from the Hall resistance data. Specifically, at a temperature of $T = 2$ K, the deduced carrier concentration and mobility stand at

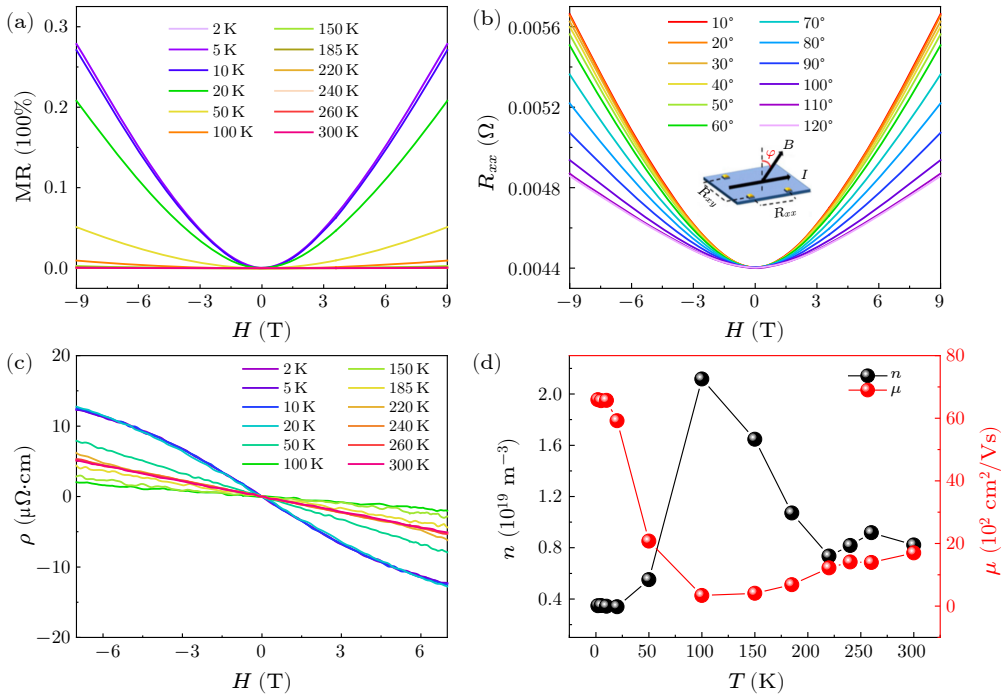

Fig. 2. (a) Magnetoresistance (MR) curves at various temperatures with the magnetic field oriented perpendicular to the ab plane. (b) Angle dependence of MR curves as the magnetic field rotates from the c axis to the ab plane at $T = 2\,\mathrm{K}$. A measurement diagram is shown in the inset. (c) Variation in the Hall resistance profile of $Bi_2Rh_3Se_2$ with magnetic field at various temperatures. (d) Temperature dependence of carrier concentration and mobility extracted from the Hall data in (c).

$3.47 \times 10^{18}\,\mathrm{m}^{-3}$ and $6.59 \times 10^{3}\,\mathrm{cm}^2/\mathrm{Vs}$, respectively. Such values are comparable to some typical topological materials such as Bi_2Se_3,[26] Sb_2Te_3,[27] $SrAs_3$,[28] suggesting the potentially realizable novel quantum effects and sensor applications in $Bi_2Rh_3Se_2$.

To investigate the in-plane transport properties of $Bi_2Rh_3Se_2$, we rotated the magnetic field within the ab plane and recorded the transverse and longitudinal voltages simultaneously, yielding the planar Hall resistance (R_{xy}^{PHE}) and the planar anisotropic resistance (R_{xx}) correspondingly. According to the PHE theory, ρ_{xx} and ρ_{xy}^{PHE} can be expressed as[29,30]

$$\rho_{xx} = \rho_{\perp} + \Delta\rho \cos^2\theta, \tag{1}$$

$$\rho_{xy}^{\mathrm{PHE}} = \Delta\rho \sin\theta\,\cos\theta. \tag{2}$$

Figure 3(a) depicts the ρ_{xy}^{PHE} of $Bi_2Rh_3Se_2$ under different magnetic fields at $T = 2\,\mathrm{K}$. The inset shows a schematic diagram of the device configuration. The difference value of resistivity is defined as $\Delta\rho = \rho_{\parallel} - \rho_{\perp}$, quantifying the variance of planar anisotropic resistance. Here, $\rho_{\perp}$ denotes the resistivity when the magnetic field within the plane is orthogonal to the current (θ equals 0° or π), and $\rho_{\parallel}$ indicates the resistivity when the magnetic field is aligned with the current (θ is $\pi/2$ or $3\pi/2$). The formulas obviously demonstrate that ρ_{xx} and ρ_{xy}^{PHE} exhibit periodic behavior with a frequency of π in relation to the angle θ. Before analyzing the data, the intrinsic PHE should be additionally validated due to some irresistible error factor throughout the measurement. (i) Because there could be a component of the magnetic field that extends beyond the plane, we ascertain the standard Hall effect apart from the ρ_{xy}^{PHE} by assessing ρ_{xy}^{PHE} with both positive and negative magnetic fields applied. We find that the ρ_{xy}^{PHE}'s in opposite field directions agree strongly with each other, which rules out the effect of normal Hall resistance. The same procedure is applied to ρ_{xx} in order to remove the effect of the ordinary magnetoresistance. (ii) The longitudinal resistance components within and perpendicular to the plane, which arise from minor longitudinal discrepancies in the Hall sensor's alignment, exhibit angular dependencies of $\cos^2\theta$ and $\cos^2(\theta + \delta)$, in that order. The contribution of the former can be excluded by symmetrizing the data with $\rho_{xy} = \frac{\rho_{xy}(\theta) - \rho_{xy}(\pi - \theta)}{2}$. The δ in the latter term depends randomly on the geometric relationship between the current and the magnetic field, thus creating some difficulties when manipulating it. Figures 3(a) and 3(c) illustrate that the valleys and peaks are located near 45° (225°) and 135° (315°), respectively, resulting in an insignificant discrepancy in the δ angle. (iii) The constant Hall resistance component is caused by the uneven thickness of the sample. It can also be eliminated by the symmetrization method described above. Following the aforementioned procedures, Figs. 3(a) and 3(c) represent the intrinsic plane Hall resistivity and the black dashed lines are the globally fitting result using Eq. (2). One can see that they agree very well with each other.

The magnitude of the planar Hall effect, denoted as $\Delta\rho$, are extracted based on the fitting curves, and their correlation with the magnetic field is depicted in Fig. 3(b). The red dashed line is the fitting result by the power-law

with an optimal power exponent of 1.70. Previous studies have suggested that the planar Hall effect originated from chiral anomaly would manifest itself as a quadratic dependence of the magnetic field on the longitudinal magnetoresistance and the planar Hall resistance.[31–34] Otherwise, they will follow a B-linear dependence when both the applied magnetic field and electric field are parallel to the tilt axis. In the latter case, however, the planar Hall resistance and longitudinal MR will show $\sin\theta$ and $\cos\theta$ angular dependence at finite magnetic field for the same configuration. Obviously, the 2θ-periodic planar Hall resistance and longitudinal MR in $Bi_2Rh_3Se_2$ reveal that they must follow quadratic B dependent behavior for the chiral anomaly mechanism. The deviation of the observed index from the theoretical value suggests that the PHE for $Bi_2Rh_3Se_2$ may originate from some other factors other than the purely chiral anomaly. To further investigate the PHE behavior of $Bi_2Rh_3Se_2$ in detail, we studied the relationship between amplitude and temperature at $H = 9\,\mathrm{T}$, as shown in Fig. 3(d). It can be seen that the amplitude $\Delta\rho$ decreases rapidly when the temperature rises from 2 K to 150 K, and decreases gradually with further warming until it almost vanishes at 300 K. In conventional chiral-anomalous semimetal materials such as Cd_3As_2,[35] the magnitude of the PHE remains relatively stable as the temperature climbs within the lower thermal spectrum. However, it drops significantly at elevated temperatures due to the effect of thermal waves. This feature, which has been documented before, is undoubtedly not aligned with the PHE patterns in $Bi_2Rh_3Se_2$.

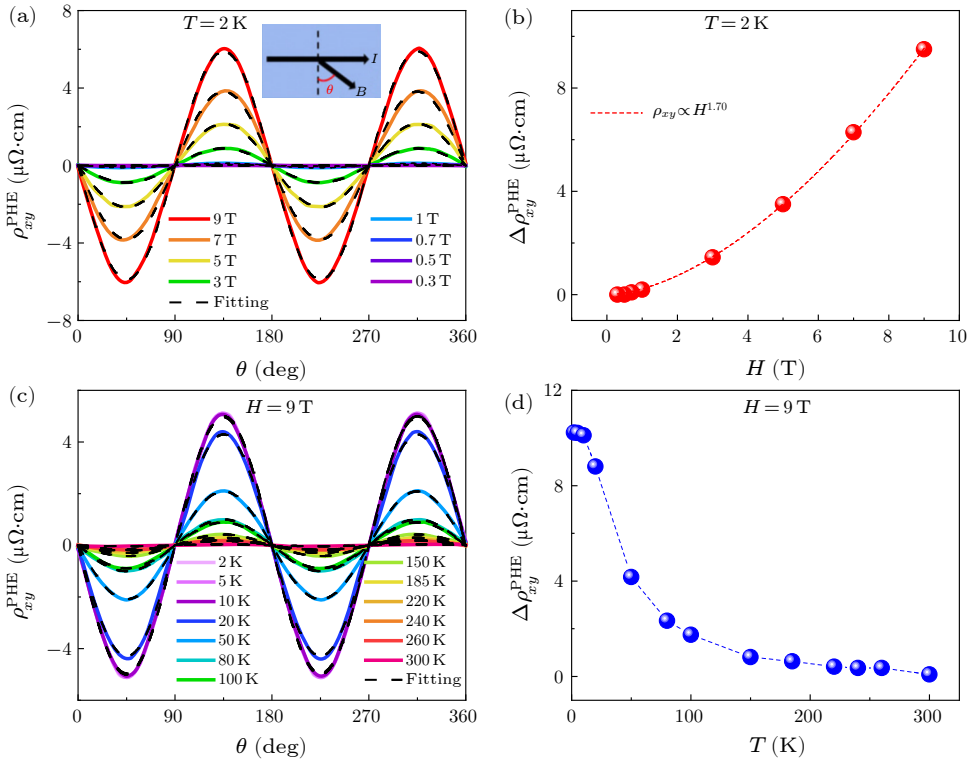

Fig. 3. (a) PHE data of $Bi_2Rh_3Se_2$ under different magnetic fields and $T = 2\,\mathrm{K}$. The black dashed lines represent the fitted curves. The inset shows a schematic diagram of the device configuration. (b) Magnetic field correlation amplitudes of PHE are extracted from the fitted curve in (a). (c) PHE data of $Bi_2Rh_3Se_2$ at different temperatures and $H = 9\,\mathrm{T}$. (d) The variation of PHE magnitude with temperature extracted from the fitted curve in (c).

Now we discuss the physical mechanism of the PHE observed in $Bi_2Rh_3Se_2$. So far, PHE behavior has been commonly discussed based on several main mechanisms. Firstly, it is a widely accepted concept that the Planar Hall effect manifests itself as a subtle effect of magnetism that is mainly noticeable in ferromagnetic materials, and originates from the coupling of spin and orbital motion of electrons.[36,37] This mechanism can be easily ruled out by us since $Bi_2Rh_3Se_2$ is a non-magnetic material. Another mechanism is the chiral anomaly and the nontrivial Berry phase, which is commonly discussed in nonmagnetic topological semimetals.[31–34,38] Considering the phenomenon of complete chiral anomaly from the standpoint of chiral anomalies, $\rho_\perp$ is expected to stay unchanged, while $\rho_\parallel$ ought to diminish as the magnetic field strengthens. The variation of $\rho_\perp$ and $\rho_\parallel$ with the magnetic field is derived from Fig. 4(a) and is depicted in Fig. 4(c). It can be seen that both of them increase markedly with increasing magnetic fields, which is different from the situation caused by chiral anomalies. Recently, in-plane anisotropic orbital magnetoresistance was also identified as a contributor to PHE in various materials with anisotropic Fermi surfaces.[39–43] Figure 4(a) shows the angle-dependent in-plane anisotropic resistivity for different magnetic fields at

$T = 2\,\mathrm{K}$. The longitudinal resistivity shows a clear π periodic trend, which can be easily described by the PHE theory of formula (1), as shown by the black dashed lines. Figure 4(b) presents the variation of $\Delta\rho_{xx}$, derived from the ρ_{xx} data in Fig. 4(a), delineated as a function of the magnetic field. It can be well fitted by $\Delta\rho_{xx} \propto H^{1.54}$ as represented by the red dashed line, and the power exponent value is close to the fitting result in Fig. 3(b), indicating a close relationship between them. Another important criterion is the orbital diagrams of ρ_{xy}^{PHE} and in-plane ρ_{xx} with angle θ as a parameter under a specific magnetic field. The orbital evolution in Fig. 4(d) plots the amplitudes of PHE and R_{xx} under different magnetic fields, with θ being the parameter. In these parameter plots, the comparison between the shock pattern and the concentric circular pattern directly reflects the peculiar nature of the PHE.[44,45] For in-plane anisotropic orbital magnetoresistance mechanism, some carrier parameters, such as mobility and effective mass, vary considerably in different directions due to anisotropy or complex Fermi pockets, leading to anisotropic orbital magnetoresistance. When an in-plane magnetic field is applied, the orbit starts at a smaller ρ_{xx} and expands to a larger ρ_{xx}, creating a shock-orbit pattern. For the chiral anomaly, the orbital diameter increases towards larger values of ρ_{xx} for higher magnetic field acquisition, associated with the transfer of quasiparticles across Landau levels with different chirality. Quasiparticle scattering can balance the charge imbalance between the chiral pockets. In this way, the parametric diagram shows concentric orbits expanding in an equilibrium pattern, producing a series of concentric circles.[44] Nonetheless, in the range of our observations, the magnetic field escalation results in the orbital path developing a shock-like pattern, which is very similar to the pattern previously reported for $HfTe_2$.[45] This phenomenon lends support to the hypothesis that anisotropic orbital magnetoresistance may be a significant factor affecting the planar Hall effect in $Bi_2Rh_3Se_2$. Although the PHE phenomenon arising from anisotropic orbital magnetoresistance mechanism has been reported in many materials, $Bi_2Rh_3Se_2$ still exhibits some different properties and provides another platform for further understanding the PHE phenomenon. Among all reported PHE nonmagnetic topological materials, $Bi_2Rh_3Se_2$ is a rare ternary compound with CDW transition and superconductivity simultaneously,[14] which facilitates our further investigation of the relationship between these quantum effects. In addition, $Bi_2Rh_3Se_2$ is a two-dimensional material with excellent air stability and easy stripping, which is extremely favorable for research of planar Hall sensors.

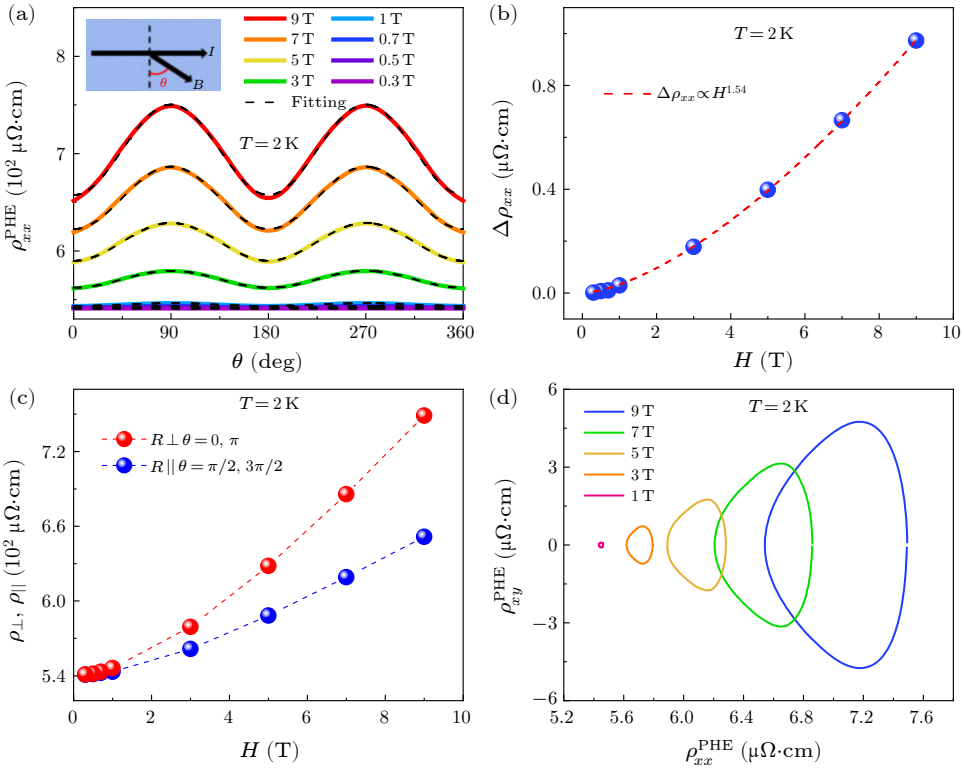

Fig. 4. (a) Angular dependence of in-plane anisotropic resistivity ρ_{xx} under different magnetic fields and $T = 2\,\mathrm{K}$. The black dashed lines are fitting curves using the PHE theory. (b) Magnetic field dependence of the $\Delta\rho_{xx}$ extracted from the fitted curves in (a). The red dashed line is a power-law fitting curve. (c) Magnetic field dependence of $\rho_\perp$ and $\rho_\parallel$ at $T = 2\,\mathrm{K}$. The red and black dashed lines represent the power law fitting results. (d) The orbits obtained by drawing ρ_{xy}^{PHE} and ρ_{xx} with angle under different magnetic fields.

In summary, we have investigated the in-plane transport properties of the ternary superconductor $Bi_2Rh_3Se_2$. The pronounced planar Hall effect, as well as the in-plane resistivity anisotropy ρ_{xx}, is clearly observed upon rotating the magnetic field with the plane of sample. Both $\rho_{xy}^{\rm PHE}$ and ρ_{xx} are well described by the classical PHE theory. Further analysis shows that the PHE is rooted in the interplay of anisotropic orbital magnetoresistance in $Bi_2Rh_3Se_2$ rather than the chiral anomaly.

Acknowledgements. This work was supported by the National Natural Science Foundation of China (Grant Nos. U19A2093, 11904002, and 12074372), the Excellent Youth Project of Natural Science Foundation of Anhui Province (Grant No. 2308085Y07).

References

[1] Keimer B and Moore J E 2017 *Nat. Phys.* **13** 1045
[2] Novoselov K S, Geim A K, Morozov S V *et al.* 2004 *Science* **306** 666
[3] Jiang K, Wu T, Yin J X *et al.* 2023 *Natl. Sci. Rev.* **10** nwac199
[4] Jiao L, Howard S, Ran S *et al.* 2020 *Nature* **579** 523
[5] Gao W S, Zhu X D, Zheng F W *et al.* 2018 *Nat. Commun.* **9** 3249
[6] Zhu A K, Wang H H, Chen Z *et al.* 2023 *Appl. Phys. Lett.* **122** 113101
[7] Neupane M, Belopolski I, Hosen M M *et al.* 2016 *Phys. Rev. B* **93** 201104
[8] Bian G, Chang T R, Sankar R *et al.* 2016 *Nat. Commun.* **7** 10556
[9] Guan S Y, Chen P J, Chu M W *et al.* 2016 *Sci. Adv.* **2** e1600894
[10] Gao W S, Zhu M C, Chen D *et al.* 2023 *ACS Nano* **17** 4913
[11] Zhu M C, Chen D, Zhu A K *et al.* 2022 *Appl. Phys. Lett.* **120** 053102
[12] Adam M L and Bala A A 2021 *J. Phys.: Condens. Matter* **33** 225502
[13] Gao T, Zhang Q, Li L *et al.* 2018 *Adv. Opt. Mater.* **6** 1800058
[14] Sakamoto T, Wakeshima M, Hinatsu Y *et al.* 2007 *Phys. Rev. B* **75** 060503
[15] Weihrich R, Matar S F, Eyert V *et al.* 2007 *Prog. Solid State Chem.* **35** 309
[16] Chen C Y, Chan C L, Mukherjee S *et al.* 2014 *Solid State Commun.* **177** 42
[17] Liu Z T, Zhang C, Wu Q Y *et al.* 2023 *Sci. China Phys. Mech. Astron.* **66** 277411
[18] Lin T, Shi L Y, Wang Z X *et al.* 2020 *Phys. Rev. B* **101** 205112
[19] Wang Y S, Chen B, Liu Z T *et al.* 2023 *Phys. Rev. B* **108** 045118
[20] Ikeda M, Zhang Z Y, Goto H *et al.* 2023 *Inorg. Chem.* **62** 7453
[21] Zhao Y F, Liu H W, Zhang C L *et al.* 2015 *Phys. Rev. X* **5** 031037
[22] Zhao Y F, Liu H W, Yan J Q *et al.* 2015 *Phys. Rev. B* **92** 041104
[23] Narayanan A, Watson M D, Blake S F *et al.* 2015 *Phys. Rev. Lett.* **114** 117201
[24] Parish M M and Littlewood P B 2003 *Nature* **426** 162
[25] Manyala N, Sidis Y, DiTusa J F *et al.* 2000 *Nature* **404** 581
[26] Kumar D and Lakhani A 2018 *Phys. Status Solidi RRT* **12** 1800088
[27] Zhang J K, Hu T J, Yan J J *et al.* 2017 *Mater. Lett.* **209** 78
[28] An L L, Zhu X D, Gao W S *et al.* 2019 *Phys. Rev. B* **99** 045143
[29] Zhong J Y, Zhuang J C, and Du Y 2023 *Chin. Phys. B* **32** 047203
[30] Zhong J Y, Yang M, Wang J F *et al.* 2024 *ACS Nano* **18** 4343
[31] Nandy S, Sharma G, Taraphder A *et al.* 2017 *Phys. Rev. Lett.* **119** 176804
[32] Shao J M and Yan L J 2023 *J. Phys.: Condens. Matter* **35** 025401
[33] Ai W, Chen F Y, Liu Z C *et al.* 2024 *Nat. Commun.* **15** 1259
[34] Ghosh S, Sinha D, Nandy S *et al.* 2020 *Phys. Rev. B* **102** 121105
[35] Wu M, Zheng G L, Chu W W *et al.* 2018 *Phys. Rev. B* **98** 161110
[36] Liu Y, Yang J Y, Chu W W *et al.* 2017 *Appl. Phys. Lett.* **111** 033103
[37] You Y R, Gong Y Y, Li H *et al.* 2019 *Phys. Rev. B* **100** 134441
[38] Ge J, Ma D, Liu Y Z *et al.* 2020 *Natl. Sci. Rev.* **7** 1879
[39] Wang H, Huang Y X, Liu H Y *et al.* 2024 *Phys. Rev. Lett.* **132** 056301
[40] Li L, Cao J, Cui C X *et al.* 2023 *Phys. Rev. B* **108** 085120
[41] Meng J C, Xue H X, Liu M R *et al.* 2020 *J. Phys.: Condens. Matter* **32** 015702
[42] Wang X R 2022 *Chin. Phys. Lett.* **39** 027301
[43] Wang P, Hou T, Tang F D *et al.* 2021 *Chin. Phys. Lett.* **38** 017201
[44] Chen F C, Luo X, Yan J *et al.* 2018 *Phys. Rev. B* **98** 041114
[45] Li Q X, Jin G J, Tang N N *et al.* 2023 *Phys. Rev. B* **108** 235155